THE ASTROPHYSICAL JOURNAL, 339:222–230, 1989 April 1

HIGH-VELOCITY FLOWS IN THE NGC 7538 MOLECULAR CLOUD

OSAMU KAMEYA, TATSUHIKO I. HASEGAWA, NAOMI HIRANO, AND KEIYA TAKAKUBO
Astronomical Institute, Tohoku University
AND
MUNEZO SEKI
College of General Education, Tohoku University
Received 1988 April 15; accepted 1988 September 13

ABSTRACT

Results of a CO ($J = 1$–0) spectral line mapping in the core of the NGC 7538 molecular cloud, measured with 16″ angular resolution, are reported. At least three high-velocity flows have been found, and their detailed characteristics are investigated. One of the new high-velocity flows is situated around IRS 9, and is about 1.6 pc × 1.6 pc in extent. This is probably a bipolar flow and has a complicated structure. The blue-shifted part of the flow delineates a reflection nebula around IRS 9 and shows a shell-like structure. The flow around IRS 1 shows a clear bipolar pattern along NW–SE line. The direction of the flow axis is not perpendicular to that of the elongation of the disk around IRS 1 and seems to change with distance from the center by ~40°. A flow near IRS 11, which has been reported in 1986 by Kameya *et al.* in the CS ($J = 1$–0) line, shows bipolar characteristics centered on IRS 11. The morphology of the flow can be explained if the high-velocity flow around IRS 11 is interacting with nearby dense ambient gas. A further flow is possibly present at the southern part of IRS 11, but it does not show clear bipolarity.

The total energy of these high-velocity flows is 4×10^{47} ergs. The energy inputs from them to the high-density core are sufficient to support the turbulent motions for at least their dynamical time scales (several 10^4 yr). This particular core region is a very active site of the high-velocity molecular outflow phenomena.

Subject headings: interstellar: molecules — nebulae: H II regions — nebulae: individual (NGC 7538) — nebulae: internal motions — stars: formation

I. INTRODUCTION

Star-forming regions frequently contain high-velocity molecular flows (e.g., Bally and Lada 1983; Lada 1985), which often show a bipolar pattern. This appearance, together with the presence of disks around protostars (e.g., Torrelles *et al.* 1983; Kaifu *et al.* 1984), gives very important observational clues for studies of the star-formation mechanism.

On the other hand, it has been suggested that T Tauri winds or high-velocity flows may excite turbulent motions in nearby molecular clouds, and then trigger the formation of the next-generation stars (Norman and Silk 1980; Campbell and Thompson 1984; Fukui *et al.* 1986). It is important to study the interaction of such high-velocity flows with the outer quiescent parts of a molecular cloud.

One of the candidates suitable for such a study is the NGC 7538 molecular cloud. Werner *et al.* (1979) showed that the high-density core region associated with NGC 7538 is a very active star-forming region, which contains five IR sources (IRS 1, 2, 3, 9, and 11) within 3′.5 × 3′.5 (equivalent to 2.7 pc × 2.7 pc at a distance of 2.7 kpc; *IAU Trans.* **12B**, 351 [1964]). Furthermore, several high-velocity flows have been detected in the core region (Fischer *et al.* 1985; Kameya *et al.* 1986, hereafter Paper I), and a large amount of energy may have been input to the ambient part of the core.

A high-velocity flow around IRS 1 was found by Bally and Lada (1983) and was studied by Campbell and Thompson (1984), and the bipolarity of the flow was shown by Fischer *et al.* (1985). Scoville *et al.* (1986) confirmed this bipolar flow and found a rotating disk around IRS 1.

Recently, Kameya *et al.* (Paper I) made CS $J = 1$–0 observations with a 33″ beam and showed that there is another prominent molecular outflow near IRS 11, and that at least three high-velocity flows are present in the core region. This suggests that the number of the flows in the core of the NGC 7538 molecular cloud is the largest among surveyed massive-star formation regions. Therefore, this region seems to be one of the most important regions to investigate the characteristics of high-velocity flows.

In this paper we report observations of the high-velocity flows in the NGC 7538 high-density core region, using flows in the NGC 7538 high-density core region, using CO $J = 1$–0 data obtained with the NRO 45 m radio telescope, with an angular resolution of 16″. The purpose of this investigation are to know (1) whether there are any high-velocity flows around IRS 9 or not, (2) whether the prominent flow near IRS 11 is actually related to IRS 11, (3) how many high-velocity flows are in the high-density core, (4) what are the characteristics of these flows, and (5) what are effects of these high-velocity flows as they interact with the outer quiescent part of the core.

We present the observational methods in § II, the results of the observations in § III, and analysis of the data and discussion of the kinematics of the high-velocity flows in § IV. Discussion of the characteristics and the effects of these flows is given in § V, and the conclusions are given in § VI.

II. OBSERVATIONS

CO $J = 1$–0 observations were made on 1985 May 9 and 10 with the NRO 45 m radio telescope[1]. The estimated FWHM of

[1] Nobeyama Radio Observatory is a branch of the National Astronomical Observatory, the Ministry of Education, Science, and Culture, Japan.

the telescope beam and the beam efficiency at 115 GHz are 16″ and 0.34. The pointing accuracy was checked once every 2 or 3 hr using the SiO ($J = 1$–0, $v = 1$ and 2) maser emission from R Cas at 43 GHz, and was estimated to be less than 6″.

The receiver frontend was a single-sideband (SSB) cryogenically cooled Schottky mixer, which had a system noise temperature T_{sys} (SSB) of 800–850 K, including contributions from atmospheric emission. For the SiO maser observations, a receiver frontend working in the 40 GHz band was used. Ten arrays of the 2048 channel Acousto-Optical Spectrometer (AOS) were used for the backends. Six of the ten arrays were operated with high-resolution, having a channel interval of 20 kHz and an effective frequency resolution of 37 kHz (0.096 km s^{-1} at 115 GHz). The mean values of seven individual AOS channels, which correspond to a velocity resolution of 0.37 km s^{-1}, are used for the present data analyses.

Two hundred positions were observed with a 15″ grid spacing, which was decreased to 10″ around IRS 1. These observed positions are shown in Figure 1. We shall use offsets (ΔR.A., Δdecl.) from IRS 1 [$\alpha(1950) = 23^h11^m36^s.8$, $\delta(1950) = 61°\ 11'48''$] to represent the observed positions.

The observations were made in the "multipoint on-off" switching mode; nine on-positions and three off-positions were observed sequentially for each scan with integration time per point of 30 s. Each scan was always started at the position of IRS 1 (0″, 0″). The peak antenna temperature of the line profile obtained at this reference position was used to calibrate the intensity scale of each scan set to remove "scanning effects." The brightness temperature of the peak line strength at IRS 1 was estimated to be 58 K. The effective integration time at each position observed was 80 s in most cases. The rms noise fluctuations averaged over seven channels were 0.26–0.65 K (typically 0.4 K).

III. RESULTS

CO line emission was detected at every observed position with a good signal-to-noise ratio (> 14). The line profiles at 121 points out of 200 points have high-velocity wings (at 0.4 K level they have velocity ranges larger than 20 km s^{-1}). Figure 2 shows the typical CO line profiles at IRS 1, IRS 9, IRS 11, and position A (see below), which have high-velocity wings, and that at (30″, −45″), which has no obvious high-velocity wing.

Figure 3 shows a schematic map of the regions which have some enhancements in integrated intensities of blue and red wings. The high-velocity wings are observed in an area of 3 pc × 3 pc which covers 57% of the measured area of the high-density core. We have found three regions in which some high-velocity flows exist close to IR sources. One of these three regions is close to IRS 9. This is the newly detected high-velocity flow associated with IRS 9. The other two regions are found near IRS 1 and IRS 11, and agree well with the positions of the CS high-velocity flows at IRS 1, positions A and D (Paper I, in which positions A and D are defined). We consider that those candidates are actually high-velocity flows, because (1) they have large velocity ranges at the 0.4 K level (> 31 km s^{-1}) and (2) three of these agree well with the positions of the CS high-velocity flows.

Figures 4*a*–4*d* show integrated intensity maps for the high-

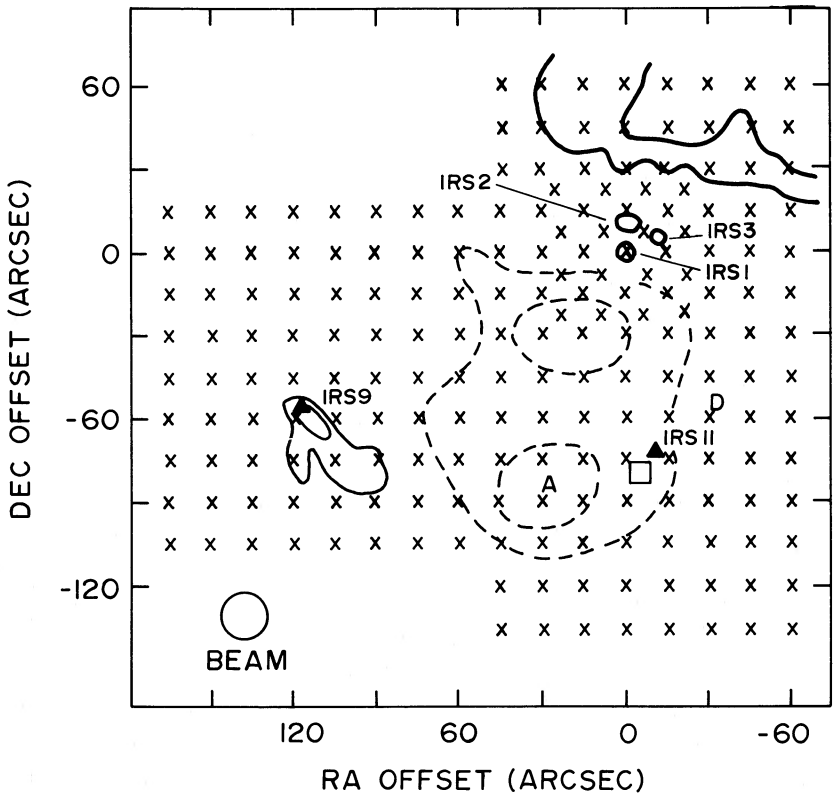

FIG. 1.—A map of NGC 7538 core region. The lowest contour of the 6 cm aperture synthesis map by Israel (1977) is indicated by thick solid lines. The IR sources 9 and 11 (Werner *et al.* 1979) and maser sources near IRS 11 are indicated by triangles and a square, respectively. The two contours of a reflection nebula around IRS 9 are shown by thin solid lines. The contours of $C^{34}S$ emission are shown by broken lines. The contour levels indicated are 0.55 K and 0.75 K. Positions A and D (see text) are shown. The offset position (0″, 0″) is at IRS 1 [$\alpha(1950) = 23^h11^m36^s.8$, $\delta(1950) = +61°11'48''$], and the observed positions are shown with crosses.

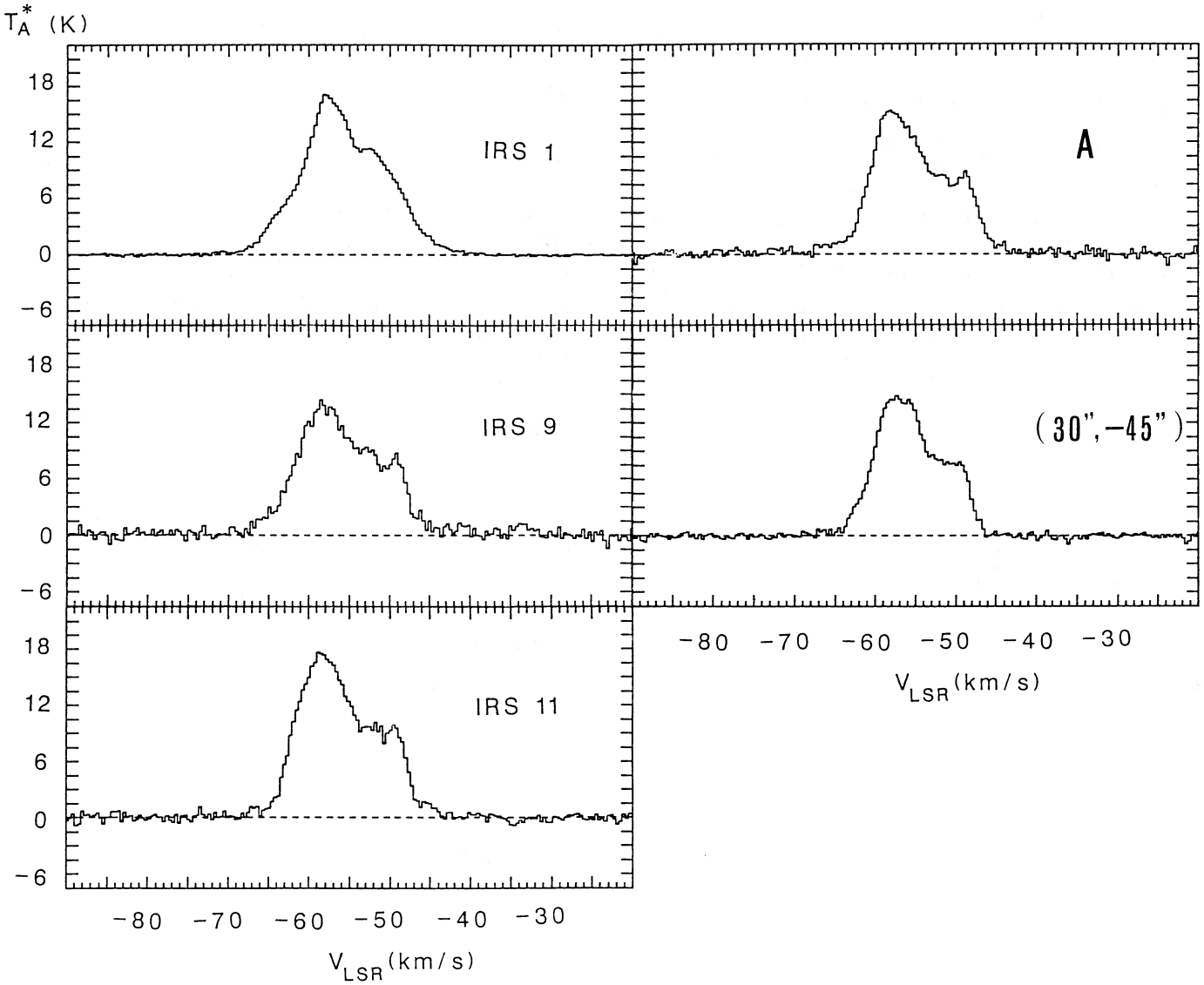

FIG. 2.—Profiles of the CO line at IRS 1 (0″, 0″), IRS 9 (120″, −60″), IRS 11 (−15″, −75″), A (30″, −90″), and (30″, −45″)

velocity flows. For Figures 4*a*, 4*b*, and 4*d* the integration ranges are -70 km s^{-1} $< V_{LSR} < -65$ km s^{-1} for the blue wings and -45 km s^{-1} $< V_{LSR} < -40$ km s^{-1} for the red wings. These velocity ranges correspond to the velocity differences of -12 to -7 km s^{-1} and 13–18 km s^{-1} from the typical quiescent-gas velocity ($V_{LSR} \sim -58$ km s^{-1}) for the blue and red wings, respectively. On the other hand, the integration ranges for Figure 4*c* are -64 km s^{-1} $< V_{LSR} < -62$ km s^{-1} for the blue wings and -48 km s^{-1} $< V_{LSR} < -46$ km s^{-1} for the red wings. These differences in integration ranges are based on the fact that the molecular outflow around IRS 11 is seen only in these lower velocity ranges (see below).

The flow around IRS 1 shows a clear bipolarity along a NW–SE direction and extends 74″ × 67″ (1.0 pc × 0.9 pc) (see Fig. 4*a*). The spatial structure of the flow is consistent with the results of Fischer *et al.* (1985) and Scoville *et al.* (1986).

The flow around IRS 9 has a large size of $>2' \times 2'$ (>1.6 pc × 1.6 pc). The blueshifted component is situated in the southeastern part of this region and the redshifted gas to the northern, eastern, and southwestern parts. Although the distribution is complex, we can find differences in the locations of the blue and red lobes (see Fig. 4*b*). Hence, this flow is probably bipolar. The most interesting fact is that the blueshifted marterial seems to delineate the reflection nebula which was found by Werner *et al.* (1979). A shell-like structure is seen in the blueshifted gas, but this is not obvious from the redshifted material. At the position (90″, −90″), both the red and blue wings are prominent suggesting that another high-velocity flow may exist at this position.

The third high-velocity flow is situated close to IRS 11 and shows a clear bipolar pattern (see Fig. 4*c*). The maximum position of the integrated intensity for each velocity range of 1 km s^{-1} of the flow around IRS 11 shifts to the southeast smoothly with increasing radial velocity from $V_{LSR} = -64$ km s^{-1} to $V_{LSR} = -56$ km s^{-1}. For the velocity of the quiescent gas ($V_{LSR} \sim -58$ km s^{-1}) the maximum position is situated at IRS 11 exactly. Hence this high-velocity flow is most likely a bipolar flow centered on IRS 11. The size of the flow is 0.8

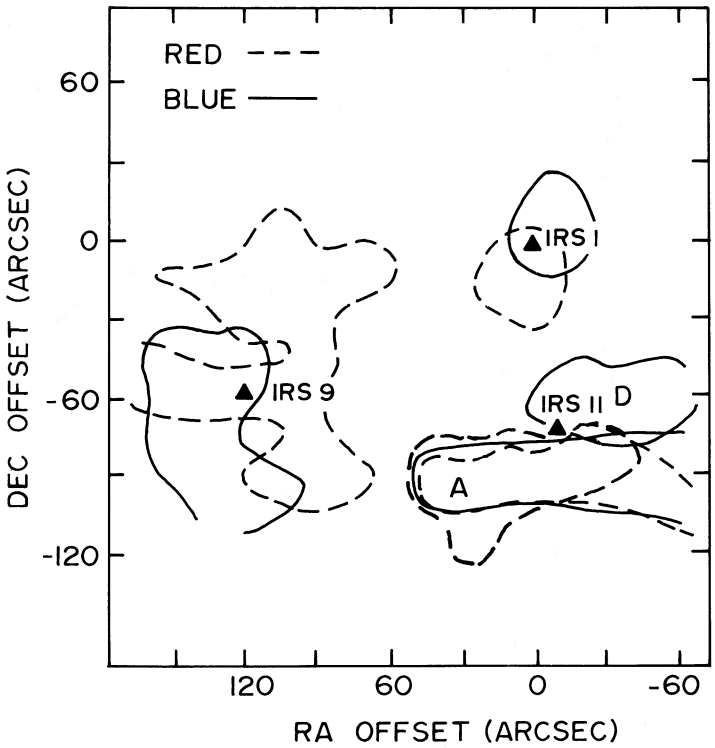

FIG. 3.—A schematic map of the high-velocity flows. Solid lines and broken lines indicate the blueshifted and redshifted parts of each flow. Velocity ranges of the integration for each flow are the same as those in Fig. 4.

pc × 0.8 pc (1′ × 1′). On the other hand, Kameya *et al.* (Paper I) have found a high-velocity CS flow at position D, lying 20″ northwest of IRS 11. Since the CS flow, which has a size of 40″, is localized within the area of the CO flow, and the flow velocities for both CO and CS lines are limited only to a low-velocity range, the flow indicated from the CS data is probably the same as that observed with the CO line. The positional deviation of the CS flow IRS 11 may be ascribed to a systematic positioning error of the CS observations of up to 20″ to the southeast of the indicated position. We are not always sure of the real distribution of the redshifted CO flow ($V_{LSR} > -55$ km s^{-1}) for two reasons. (1) A cloud ($V_{LRS} = -49 \pm 2$ km s^{-1}) is situated on the same line of sight to the high density core. Hence, this cloud component probably blends with the red wing due to the high-velocity flow of IRS 11 (Campbell and Thompson 1984). (2) The high-velocity flow near position A, which is situated southeast of IRS 11, blends with the redshifted flow of IRS 11 (see below). In order to know the distribution of each high-velocity flow, additional observations using the optically thin ^{13}CO ($J = 1$–0) line will be necessary.

Figure 4*d* indicates that the bluer and the redder parts of the flow lie 15″ south of IRS 11, elongated along an east-west direction, and have a size of 105″ × 30″ (1.4 pc × 0.4 pc). The distribution of integrated intensity of the redshifted and blueshifted wings is similar and shows no obvious bipolarity. The elongation of this CO high-velocity region may be partly due to poor baseline subtraction of the data at the positions (15″, −90″), (−30″, −90″), and (−45″, −90″). From these results we cannot deny all the possibilities that this region is a part of the substructure of the third flow. However, there are some suggestions of this high-velocity region being distinct from this third flow as follows. (1) The blueshifted part of the region is seen to the south of IRS 11, but that of the third flow is seen to the north of it. (2) As mentioned above, the third flow seems to have the clear bipolar pattern. (3) Comparing the distribution of the high-velocity CO with that of CS (Paper I), we find that the eastern side of the CO flow corresponds to the position A (30″, −90″), a maximum point in the map of integrated intensity of the CS wings. Considering the relative positioning error of our CO observations, ±6″, and that of Paper I, this high-velocity CO flow is possibly the same as the high-velocity CS flow at position A and is possibly the fourth high-velocity flow.

The observed parameters of these high-velocity flows are summarized in Table 1. D_{max} and D_{min} indicate the sizes of these flows along the major and minor axes, respectively. All high-velocity flows are of order of 1 pc × 1 pc in size. The collimation factors, $CF = D_{max}/D_{min}$, for the three high-velocity flows except for the flow at position A are about unity. This suggests that either the major axes of these high-velocity flows are nearly parallel to the line of sight, or that these flows are not highly collimated. The LSR velocities, V_{red} and V_{blue}, at which the intensities of the high-velocity wings become 0.4 K, and the half-velocity extents of the flows, $\Delta V = (V_{red} - V_{blue})/2$, are also given in Table 1. The half-velocity extents of the high-

TABLE 1

OBSERVED PARAMETERS OF THE HIGH-VELOCITY FLOWS

REGION	D_{max} (pc)	D_{min} (pc)	CF	V_{LSR} Blue (km s^{-1})	V_{LSR} Red (km s^{-1})	ΔV (km s^{-1})
IRS 1	1.0	0.9	1.1	−76	−37	20
IRS 9	1.6	1.6	1.0	−72	−33	20
IRS 11	0.8	0.8	1.0	−69	−38	17
A	1.3	0.4	3.3	−74	−31	22

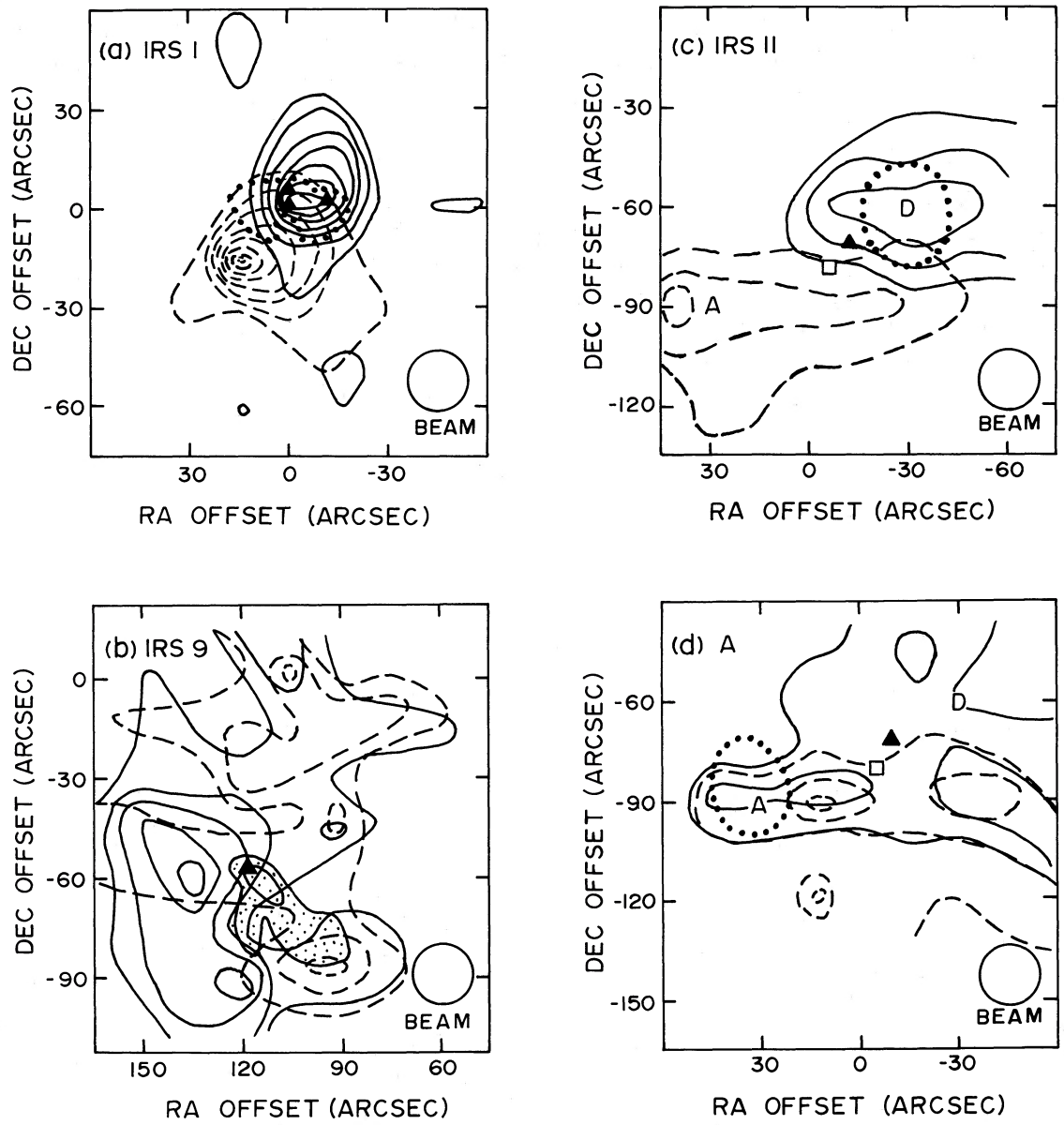

FIG. 4.—Maps of CO integrated intensity in blueshifted and redshifted high-velocity parts. Solid lines and broken lines indicate the blueshifted and redshifted parts, respectively. (*a*) The flow at IRS 1 region. The blue wing is integrated from -70 km s^{-1} to -65 km s^{-1}, and the red wing from -45 km s^{-1} to -40 km s^{-1}. Contour levels for the blue and red wings are 3, 4.5,... K km s^{-1} and 1.5, 3,... K km s^{-1}, respectively. The rotating disk around IRS 1 suggested by Scoville *et al.* (1986) is shown by a dotted line, and the IR sources 1, 2, 3 (Werner *et al.* 1979), are shown by triangles. (*b*) The flow at IRS 9 region. The ranges of the integration are the same as those of (*a*). Contour levels for both blue and the red ones are 1.5, 3,... K km s^{-1}. IRS 9 is indicated by a triangle. The reflection nebula around IRS 9 found by Werner *et al.* (1979) is shown by thin solid lines and dots. (*c*) The flow at IRS 11 region. The blue wing is integrated from -64 km s^{-1} to -62 km s^{-1}, and the red wing from -48 km s^{-1} to -46 km s^{-1}. Contour levels for the blue and red wings are 10.5, 12, 13.5 K km s^{-1} and 6, 7.5, 9 K km s^{-1}, respectively. IRS 11 and the maser sources near IRS 11 are indicated by a triangle and a square, respectively, and the dotted circle indicates the half power contour of the CS high-velocity flow at position D (Paper I). (*d*) The flow at position A. The integration ranges and contour levels are the same as those of (*b*). The triangle and square are the same as those of (*c*), and the dotted circle indicates the CS high-velocity flow at position A (Paper I).

velocity flow of IRS 11 are smaller than those values of the other three high-velocity flows. This tendency is consistent with the fact that the flow at IRS 11 is restricted to the lower velocity range.

IV. KINEMATICS

In this section we derive physical quantities of the four high-velocity flows, such as their mass, momentum, and energy. These parameters for each flow are given in Table 2. Since no ^{13}CO data were available for the high-velocity wings, we have estimated column densities of the high-velocity flows by using only the ^{12}CO data, assuming that they are optically thin and that their excitation temperatures are equal to those of main components. These values may contain a rather large amount of uncertainty, because of the ambiguities in the optical depth, the inclination angles of the actual flow axes to the line of sights, the velocity integration intervals, ^{12}CO relative abundance, and T_{EX} of the high-velocity flow gas. These values, however, probably do not differ from the actual values by more than an order of magnitude.

TABLE 2

PHYSICAL PARAMETERS OF THE HIGH-VELOCITY FLOWS

Region	M_{hv} ($M_\odot$)	P_{hv} (10^{40} g cm s^{-1})	E_{hv} (10^{46} ergs)	t_{hv} (10^4 yr)	F_{hv} (10^{28} dyn)	L_{hv} (10^{34} ergs s^{-1})	$\dot{M}_*$ (10^{-4} $M_\odot$ yr^{-1})	L_* (10^4 $L_\odot$)	L_{hv}/L_*	cF_{hv}/L_*
IRS 1	16	6	6	2.4	9	9	1	15	5×10^{-4}	4
IRS 9	34	10	10	4.1	10	10	2	3	1×10^{-3}	32
IRS 11	16	5	4	2.4	7	6	1	1	2×10^{-3}	57
A	11	5	5	3.0	5	5	0.8	...	...	...

The column density of the CO high-velocity gas in an LTE state can be estimated as

$$N(^{12}\mathrm{CO}) = \frac{4.2 \times 10^{13} T_{EX}}{\exp(-5.5/T_{EX})} \int T_R \, dV \ \mathrm{cm}^{-2}, \quad (1)$$

where T_{EX} is the excitation temperature in degrees Kelvin (K), $T_R = T_A^*/\eta_B$ is the brightness temperature in K, and V is the velocity width in units of km s^{-1} (e.g., Goldsmith *et al.* 1984). The ranges of integration for the blue and the red wings are (-70 to -60) km s^{-1} and (-47 to -37) km s^{-1}, respectively. These ranges do not contain emission from the small component at $V_{LSR} \sim -49$ km s^{-1} corresponding to a line-of-sight cloud. T_{EX} is assumed to be 35 K in this case based on the gas kinetic temperature derived by Fischer *et al.* (1985). Assuming the ^{12}CO relative abundance to be 1×10^{-4}, the total column density of the high-velocity gas is given by

$$N(\mathrm{H_2}) = 1.7 \times 10^{19} \int T_R \, dV \, \mathrm{cm}^{-2}. \quad (2)$$

The derived values of $N(H_2)$ of the high-velocity flows at IRS 1, IRS 9, IRS 11, and position A, are then 1.7×10^{21}, 1.1×10^{21}, 2.2×10^{21}, and 1.7×10^{21} cm^{-2}, respectively.

The total mass of material in the flow, M_{hv}, is estimated from $N(H_2)$ and the observed area of high-velocity flow. The derived masses are in the range of 14–15 $M_\odot$ for the filling factor of unity. Using the flow velocity ΔV in Table 1, the flow momentum, P_{hv}, and the flow energy, E_{hv}, are calculated using the relationship $P_{hv} = M_{hv} \Delta V$ and $E_{hv} = \frac{1}{2} M_{hv} \Delta V^2$, respectively. The energy of each high-velocity flow is (0.6–1.7) $\times 10^{47}$ ergs. The energy summed up over the four flows becomes about 3.7×10^{47} ergs, suggesting that the high-density core in the NGC 7538 molecular cloud is one of the most active regions of outflows similar to those associated with S140 and NGC 2071 (see, e.g., Bally and Lada 1983).

The dynamical time scale of the high-velocity flow, t_{hv}, is estimated by $t_{hv} = D_{max}/\Delta V$, although this time scale depends on the angle between the major axis of the high-velocity flow and the line of sight. Using t_{hv}, the force and mechanical luminosity required to drive the flow are estimated by $F_{hv} = P_{hv}/t_{hv}$ and $L_{hv} = E_{hv}/t_{hv}$, respectively. The efficiency of energy input from the the central infrared object to the high-velocity flow is estimated as L_{hv}/L_*, where L_* is the luminosity of the infrared source (IRS 1, 9, or 11). The derived values of the efficiency of the energy input are (0.2–2.0) $\times 10^{-3}$, similar to those estimated for other sources (e.g., Bally and Lada 1983).

The ratio of momentum input from the central protostar to that of the high-velocity flow, cF_{hv}/L_*, for the flows around IRS 1, IRS 9, and IRS 11 are ~ 6, ~ 43, and ~ 75, respectively[2]. The derived values of this ratio for IRS 9 and IRS 11 are in a range found for other high-velocity flows by Lada (1985), of 10–1000. Thus, radiation pressure is not effective as a supply of energy to drive these high-velocity flows. On the other hand, the contribution of the radiation pressure from IRS 1 is rather significant for acceleration of this high-velocity flow, because the ratio, ~ 6, is closer to one.

The mass flux is estimated as $\dot{M}_* = P_{hv}/(t_{hv} \Delta V_w)$ assuming these flows are driven by stellar wind having a velocity of $\Delta V_w \sim 100$ km s^{-1} (Goldsmith *et al.* 1984; Snell *et al.* 1984) and are $\dot{M}_* = (1\text{–}2) \times 10^{-4} \, M_\odot \, \mathrm{yr}^{-1}$, almost equal to those of other high-velocity flow sources (e.g., Snell *et al.* 1984).

V. DISCUSSION

The large high-velocity flow found with CO lines using a 66″ beam in the NGC 7538 high-density core by Campbell and Thompson (1984), is resolved to four high-velocity flows: those around IRS 1, IRS 9, IRS 11, and position A.

First, we discuss characteristics of each flow and then the energy supply from the high-velocity flows into the high-density core region.

a) The Flow at IRS 9 Region

The size of this high-velocity flow is very large (1.6 pc × 1.6 pc; see Fig. 4*b*). The most interesting characteristics are that a blueshifted part of the flow is situated on the south of IRS 9 and delineates a reflection nebula previously found at 2 μm in the southwest of IRS 9 (Werner *et al.* 1979). Tokunaga, Lebofsky, and Rieke (1981) observed the polarization of this reflection nebula at 3 μm and found that the distributions of the direction and degree of the polarization were suggestive of a normal reflection nebula. Since this nebula is seen on the optical CCD image (Campbell and Persson 1988; Eiroa, Lenzen, and Gomez 1988), the visual extinction of this region is not so large as to completely obscure the optical emission.

The coexistence of the reflection nebula and the shell in the blueshifted part of the high-velocity flow near the IR source indicates that this high-velocity flow resembles these at R Mon and at L1551 (Cantó *et al.* 1981; Snell, Loren, and Plambeck 1980).

Next we argue for the existence of a disk around IRS 9. The brightness of the reflection nebula, which has been observed in the optical CCD image at the south of IRS 9, sharply decreases toward the north. We can see that the reflection nebula is rather associated with the blueshifted flow. This suggests that only the near side of the flow in the reflection nebula is visible, but not at the back, because of the extinction due to a disk (around IRS 9). This is supported by the infrared observation (Werner *et al.* 1979) that a region of high visual extinction exists at the north and east of IRS 9, and that this visual extinction may be 15–20 mag at IRS 10 which is at 1′ northeast of IRS 9. This is also supported by the fact that A_v for IRS 9 is larger than 25.4 mag (Eiroa, Lenzen, and Gomez 1988). Therefore, we infer that a disk exists around IRS 9 and which

[2] The ratio for the IRS 1 flow is reanalyzed by using ^{13}CO ($J = 1$–0) data (Kameya *et al.* 1989) and the ^{12}CO ($J = 1$–0) data. The derived value is 4–14 which is consistent with the result using only the ^{12}CO line data.

obscure the infrared radiation coming from parts of the reflection nebula at the back of the disk. Campbell and Persson (1988) and Eiroa, Lenzen, and Gomez (1988) found a dark lane between the two diffuse nebulae on the CCD images, and they suggested the presence of a thick circumstellar disk (or torus) oriented NE–SW on the sky. However, a contour map of the peak antenna temperature of the CO line (Fig. 1 of Kameya and Takakubo 1988) indicates that the bright region around IRS 9 is elongated east-west. Maps obtained by the NRO 45 m radio telescope (Kameya *et al.* 1989) show that the contours of ^{13}CO, HCO^+, and HCN lines [tracers of dense gas; $n(H_2) > 10^4$ cm^{-3}] are very similar to the shape of the CO bright region around IRS 9. Some velocity gradients toward east-west directions have also been found by the ^{13}CO observations (Kameya *et al.* 1989). Therefore the disk around IRS 9 is probably oriented east-west on the sky and the dark lane between the two diffuse nebulae may be a substructure of the disk.

This region has no compact H II regions. However, $v = 1$–0 $S(1)$ line emission from H_2 was detected at the position of the reflection nebula by Fischer *et al.* (1980) with a 34″ beam. This emission is caused by collisional excitation in the high-velocity gas heated (to $\sim$2000 K) by a shock of the high-velocity flow at IRS 9 and/or an excitation caused by ultraviolet radiation from IRS 9. In addition to this, the $v = 1$–0 $S(1)$ emission was also detected at IRS 1 (Fischer *et al.* 1985). Therefore the existence of the H_2 emission at both the IRS 1 and IRS 9 regions suggests that a similar mechanism is working in both regions.

b) *The Flow at IRS 1 Region*

The CO high-velocity flow is elongated 0.3 pc from IRS 1 in a NW–SE direction with a position angle of 140°. However, VLA continuum observations by Campbell (1984) showed position angles of 165° and 180° for the central 2″ (0.03 pc) and 0.3″ (0.005 pc or 10^3 AU) regions, respectively. These results indicate that the position angle of the high-velocity flow decreases away from IRS 1.

On the other hand, Scoville *et al.* (1986) suggested the presence of a rotating disk with a mass of 100–500 $M_\odot$ which is elongated in an east-west direction. This disk has been confirmed by the following observational results: (1) the "peanut" structure of ionized gas smaller than 65 AU in the central region (Campbell 1984); (2) elongation of the emitting dust region toward the east and west found in a 5 μm infrared map (Hackwell, Grasdalen, and Gehrz 1982); and (3) the 162° position angle and 11% degree of polarization in the infrared with a 1″–2″ beam (Dyck and Capps 1978). Therefore this disk is perpendicular to the flow in the scale of 10^3 AU, but is not always perpendicular to it in the scale of 10^5 AU.

Now we consider the interpretation of the change of the position angle. If both the CO and radio continuum flows have flowed out along a line perpendicular to the disk, and if direction of the disk has changed with time, this change of the position angle seems to be explained at first sight. However, since the dynamical time scales of the flow in the central region (0.03 pc) and the outer region (0.3 pc) are estimated to be 10–10^2 yr and 2×10^4 yr, respectively, each part of the flow should have rotated $\sim$20° within different time scales (with a degree of difference of more than two orders of magnitude). Hence it is difficult to explain this difference of the time scales with some mechanisms which require a change of position angle such as disk precession proposed by Fukue and Yokoo (1986).

One possible explanation is that the high-velocity flow, which originally formed toward the north and the south of the center for 2×10^4 yr, has gradually changed its direction due to an increase of the ambient gas density toward northeast and southwest. When the flow interacted with the dense gas, the flow was pushed by the gas and changed the direction of the flow and flowed toward a lower density region. This idea does not contradict the fact that IRS 2 and the optical H II region NGC 7538 are situated 10″ and 30″ north of IRS 1, respectively, and the gas density increases mostly toward the north. Furthermore, 40″ southwest of IRS 1 is a blueshifted part of the high-velocity flow around IRS 11, suggesting that some density enhancements around the flow may result from an interaction with it. This density increase is consistent with the change of the flow direction toward the south.

Another possible explanation is a coupling of the gas with a large-scale magnetic field around IRS 1. The magnetic field around IRS 1 may have a direction similar to the direction of interstellar polarization near the NGC 7538 region, which orients east-west (Hall 1958). The magnetic field will have some effects on orienting and maintaining collimation of neutral outflows with sufficiently large ionization fractions. Some protostellar disks may have formed due to collapse along some magnetic fields. Nevertheless, the disk around IRS 1 may not have suffered the effect of the magnetic fields but an effect of the shock due to expansion of the H II region (Paper III) or that of the galactic rotation (Yamashita 1987), because the disk is nearly parallel to the shocked region around the NGC 7538 H II region (Paper III) and is nearly parallel to the galactic plane. Hence it is possible that the disk around IRS 1 has formed elongated toward the east-west direction and that the bipolar flow which originated perpendicular to the disk has changed its direction along the direction of the magnetic field.

c) *The Flow at IRS 11 Region*

The high-velocity flow in this region is probably a bipolar flow centered at IRS 11. The characteristics of this high-velocity flow are as follows.

1. The half-velocity extents ΔV of the wings of CO and CS lines are 16 km s^{-1} and 11 km s^{-1}, respectively. These two values are similar to but smaller than those of the other three flows. These values suggest that this flow does not contain high-velocity gas of $\Delta V > 16$ km s^{-1} and that both CO and CS emission arises in the same region in the high-velocity flow. Nevertheless, note that the ΔV is projected velocity and may be comparable to the others if the projection is corrected.

2. The CS wings are very prominent as metioned above (Paper I), suggesting that the CS abundance in the high-velocity flow is enhanced by one or two orders of magnitude as in the case of NGC 2071 (Takano 1986).

3. The visual extinction, A_V, of IRS 11 is probably several hundred magnitudes (Werner *et al.* 1979), suggesting that the high-velocity flow is embedded in the core and may be surrounded by high-density gas.

4. OH and H_2O masers are located 11″ (0.15 pc) southeast of IRS 11 (Forster *et al.* 1978). This positional difference is about 10 times larger than that of the masers close to IRS 1 (0.01 pc).

These characteristics may be explained by a high-velocity flow in a high-density gas cloud, in which the flow is hindered by the denser material. In such a situation, the flow size and velocity may not increase, in spite of large energy and momentum supplied by the central energy source. The low-velocity flow ($\sim$10 km s^{-1}) probably experiences the shock phenomenon, which enhances its CS abundance by about the order of 2

(Mitchell 1984). The absence of Brγ and H_2 vibrationally excited line emission in this region (Fischer *et al.* 1980) is not a serious problem, because their upper limit is considerably high.

IRS 11 source is not a radio continuum source but is possibly accompanied by a 2 μm reflection nebula similar to IRS 9 (Werner *et al.* 1979). These situations suggest that both the high-velocity flows around IRS 9 and IRS 11 resemble that of R Mon (Cantó *et al.* 1981) and are very different from that of IRS 1.

d) The Flow at Position A

The high-velocity flow around position A is an unusual flow, because no IR sources have been found in this region. Since a part of this flow seems to be situated in the central region of the high-density core (indicated by "A" in Fig. 4*d*), the absence of IR sources may be due either to a high visual extinction (several hundred magnitudes; Werner *et al.* 1979) of some embedded IR sources or due to a lower IR luminosity than the sensitivity limits of previous observations. The details of this flow are still uncertain because this flow is contaminated by the flows of IRS 11, and because the data quality is poor for a part of this area.

e) A Total Image

In Figure 5 we summarize the geometry of the high-velocity flows by taking a cross section through the high-density core region on a NW–SE line through IRS 1. The four high-velocity flows are shown in this figure. Since we do not know the real positions of these high-velocity flows in the core along the line of sight, we have estimated the positions by taking account of the visual extinction for each flow region.

f) Energy Supply from the High-Velocity Flows to the Turbulent Motions

The total energy of the high-velocity flows in the core region, 3.7×10^{47} ergs, is the same order as the turbulent energy of 4×10^{47} ergs in the high-density core (see below). In addition, the dynamical time scale of the flow (several 10^4 yr) is nearly comparable with the age of the optical H II region NGC 7538 (10^5 yr; Dickel, Dickel, and Wilson). Hence these high-velocity flows are intimately related to the high-density core region. Now we examine whether these high-velocity flows can supply sufficient energy to compensate for the dissipation of the turbulent energy in the high-density core.

Since the high density core region near NGC 7538 has a size $L \sim 3$ pc and a mean turbulent velocity of 2.5 km s^{-1} (Paper I), the decay time scale of the turbulence is 3 pc/2.5 km s^{-1} = 1×10^6 yr. Using the total core mass of 6000 $M_\odot$ (Paper I) and the mean turbulent velocity, we estimate the total turbulent energy is 4×10^{47} ergs and the energy dissipation rate to be 1×10^{34} ergs s^{-1}. On the other hand, the energy input by the high-velocity flows to the core is $\dot{E} \sim 4 \times 10^{35}$ ergs s^{-1}. Therefore, if the conversion efficiency is greater than 3%, the high-velocity flows can supply sufficient energy and compensate for the turbulent dissipation, at least for the dynamical time scale of the flows (several 10^4 yr). If all the flows are driven by the $\boldsymbol{J} \times \boldsymbol{B}$ force such as proposed by Uchida and Shibata (1984), the conversion efficiency is probably nearly 100% (Shibata 1987). In this case, the high-velocity flows may input enough energy not only to compensate the dissipation of the turbulent energy in the high-density core but also to destroy the core.

Norman and Silk (1981) proposed a cyclic star-formation mechanism induced by T Tauri winds. In our case the energy input is due not to the T Tauri winds but to high-velocity flows. The energy sufficient to trigger the formation of a next generation of stars, but the dynamical time scale of the flows (several 10^4 yr) is very much shorter than that of a T Tauri wind ($\sim 10^6$ yr) and may be too short to result in such triggering. How long these activities continue is a serious problem.

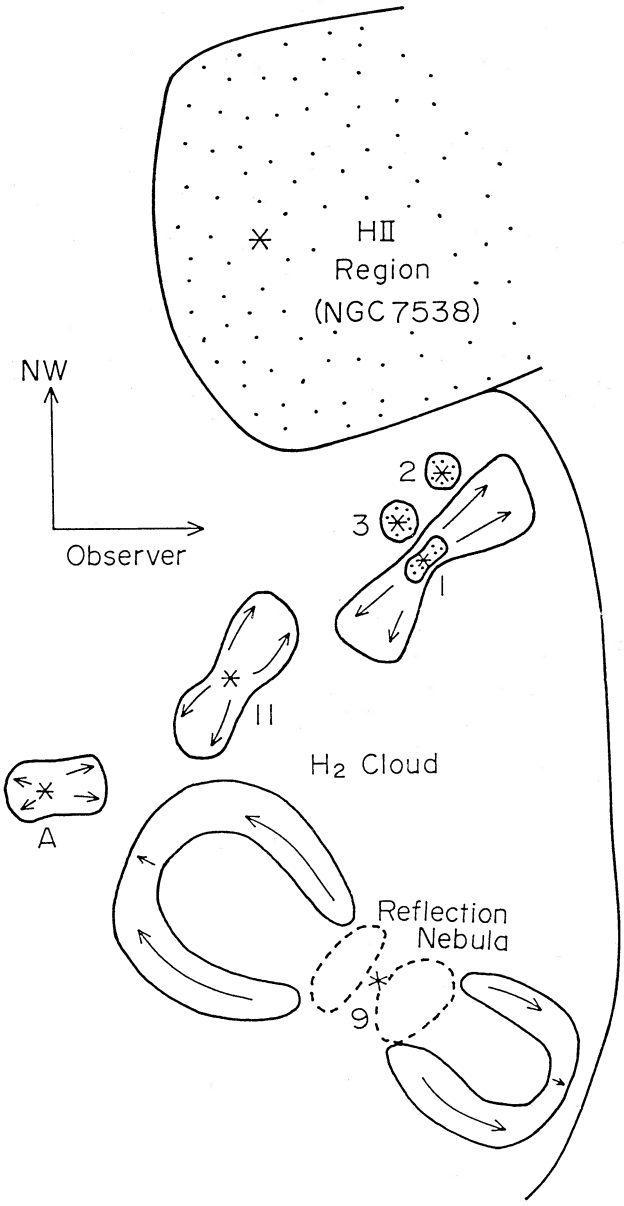

FIG. 5.—An artistic conception of the configuration of the high-velocity flows in the core region. The dotted areas indicate H II regions.

VI. CONCLUSIONS

1. The high-density core of the NGC 7538 molecular cloud is a very active site of the high-velocity flows. Three high-velocity flows and one possible candidate have been found in the core region. Three of these flows are associated with IRS 1, IRS 9, and IRS 11, and are probably bipolar. The energy input from these four high-velocity flows to the core region is so large that it can compensate the energy dissipation by turbulence in the core region for at least several 10^4 yr. Furthermore, if the

conversion efficiency is nearly 100%, these high-velocity flows will destroy the core region.

2. The high-velocity flow close to the IRS 9 region has a size of about 1.6 pc × 1.6 pc. The blueshifted part of the flow delineates the reflection nebula around IRS 9 and has a shell structure. These structures resemble the bipolar flows seen toward the R Mon and L1551 regions. There are some suggestions of the existence of a disk around IRS 9. Additional observations of confirming the existence of the disk is necessary to understand the mechanism of the disk-flow system of this region.

3. In the IRS 1 region, a clear bipolar pattern is seen along a NW–SE direction. The flow axis seems to change continuously from the flow center to the edge of the flow by approximately 40°. If both the CO flow and the radio continuum flow have flowed out along a line perpendicular to the disk, then it cannot be attributed to any rotation of the flow sources or to precession of the disk.

4. In the IRS 11 region, the velocity range of the outflowing gas is only 16 km s^{-1} and resembles that of the CS line wings. These characteristics are explained by an existence of a high-velocity flow hindered by the dense ambient gas around IRS 11.

5. In a region around position A (40″ southeast of IRS 11) both the blue and red wings are seen to the west of position A and south of IRS 11 but do not show bipolarity. Since no infrared sources have been found in this region, additional more sensitive infrared observations of this region are desired.

It is our pleasure to acknowledge many useful comments with Drs. S. Deguchi, Y. Fukui, T. Tosa, and G. White. We would like to thank the staff of NRO for the operation of the 45 m telescope during our observations and for support in the data reduction, we thank Dr. Tetsuo Hasegawa for helpful comments. We also thank Dr. Belva G. Campbell for communicating information on the CCD image of this region and for careful reading and useful suggestions as a referee. Our thanks go to Miss M. Nakamura for drawing most of the figures.

REFERENCES

Bally, J., and Lada, C. J. 1983, *Ap. J.*, **265**, 824.
Campbell, B. 1984, *Ap. J. (Letters)*, **282**, L27.
Campbell, B., and Persson, S. E. 1988, *A.J.*, **95**, 1185.
Campbell, B., and Thompson, R. I. 1984, *Ap. J.*, **279**, 650.
Cantó, J., Rodríguez, L. F., Barral, J. F., and Carral, P. 1981, *Ap. J.*, **244**, 102.
Dickel, H. R., Dickel, J. R., and Wilson, W. J. 1981, *Ap. J. (Letters)*, **250**, L43.
Dyck, H. M., and Capps, R. W. 1978, *Ap. J. (Letters)*, **220**, L49.
Eiroa, C., Lenzen, R., and Gomez, A. I. 1988, *Astr. Ap.*, **190**, 283.
Fischer, J., Righini-Cohen, G., Simon, M., Joyce, R. R., and Simon, T. 1980, *Ap. J. (Letters)*, **240**, L95.
Fischer, J., Sanders, D. B., Simon, M., and Solomon, P. M. 1985, *Ap. J.*, **293**, 508.
Forster, J. R., Welch, W. J., Wright, M. C. H., and Baudry, A. 1978, *Ap. J.*, **221**, 137.
Fukue, J., and Yokoo, T. 1986, *Nature*, **321**, 841.
Fukui, Y., Sugitani, K., Takaba, H., Iwata, T., Mizuno, A., Ogawa, H., and Kawabata, K. 1986, *Ap. J. (Letters)*, **311**, L89.
Goldsmith, P. F., Snell, R. L., Hemeon-Heyer, M., and Langer, W. D. 1984, *Ap. J.*, **286**, 599.
Hackwell, J. A., Grasdalen, G. L., and Gehrz, R. D. 1982, *Ap. J.*, **252**, 250.
Hall, J. S. 1958, *Pub. US Naval Obs.*, Vol. **17**, Part 6.
Israel, F. P. 1977, *Astr. Ap.*, **59**, 27.
Kaifu, N., *et al.* 1984, *Astr. Ap.*, **134**, 7.
Kameya, O., *et al.* 1986, *Pub. Astr. Soc. Japan*, **38**, 793 (Paper I).
Kameya, O., Hirano, N., Umemoto, T., and Takakubo, K. 1989, in preparation.
Kameya, O., and Takakubo, K. 1988, *Pub. Astr. Soc. Japan*, **40**, 413 (Paper III).
Lada, C. J. 1985, *Ann. Rev. Astr. Ap.*, **23**, 267.
Mitchell, G. F. 1984, *Ap. J.*, **287**, 665.
Norman, C., and Silk, J. 1980, *Ap. J.*, **238**, 158.
Scoville, N. Z., Sargent, A. I., Sanders, D. B., Claussen, M. J., Masson, C. R., Lo, K. Y., and Phillips, T. G. 1986, *Ap. J.*, **303**, 416.
Shibata, K. 1987, private communication.
Snell, R. L., Loren, R. B., and Plambeck, R. L. 1980, *Ap. J. (Letters)*, **239**, L17.
Snell, R. L., Scoville, N. Z., Sanders, D. B., and Erickson, N. R. 1984, *Ap. J.*, **284**, 176.
Takano, T. 1986, *Ap. J. (Letters)*, **200**, L85.
Tokunaga, A. T., Lebofsky, M. J., and Rieke, G. H. 1981, *Astr. Ap.*, **99**, 108.
Torrelles, J. M., Rodríguez, L. F., Cantó, J., Carral, P., Marcaide, J., Moran, J. M., and Ho, P. T. P. 1983, *Ap. J.*, **273**, 214.
Uchida, Y., and Shibata, K. 1984, *Pub. Astr. Soc. Japan*, **36**, 105.
Werner, M. W., Becklin, E. E., Gatley, I., Matthews, K., Neugebauer, G., and Wynn-Williams, C. G. 1979, *M.N.R.A.S.*, **188**, 463.
Yamashita, T. 1987, Ph.D. thesis, Kyoto University.

TATSUHIKO I. HASEGAWA: Department of Astronomy, St. Mary's University, Halifax, Nova Scotia B3H 3C3, Canada

NAOMI HIRANO and OSAMU KAMEYA: Nobeyama Radio Observatory, National Astronomical Observatory, Nobeyama, Minamisaku, Nagano 384–13, Japan

MUNEZO SEKI: College of General Education, Tohoku University, Sendai 980, Japan

KEIYA TAKAKUBO: Astronomical Institute, Tohoku University, Sendai 980, Japan